5-*Exo*-Cyclizations of Pentenyliminyl Radicals: Inversion of the *gem*-Dimethyl Effect

Fernando Portela-Cubillo,[†] Rafael Alonso-Ruiz,[‡] Diego Sampedro,[‡] and John C. Walton*[,†]

School of Chemistry, University of St. Andrews, EaStChem, St. Andrews, Fife, KY16 9ST, U.K., and Departamento de Química, Universidad de La Rioja, Grupo de Síntesis Química de La Rioja, Unidad Asociada al CSIC, Madre de Dios, 51, 26006, Logroño, Spain

Received: May 22, 2009; Revised Manuscript Received: August 5, 2009

This paper describes how the rates of 5-*exo*-ring closures of unsaturated iminyl radicals to pyrrolomethyl radicals respond to substituents in the pentenyl chain and at the C═N bond. Benzyl- and acyl oxime esters, as well as dioxime oxalates, were identified as suitable iminyl radical sources for electron paramagnetic resonance (EPR) spectroscopy. Pentenyliminyl radicals with aryl substituents at their C═N bonds, and one with an alkyl substituent at its C═N bond, were studied in solution by steady-state continuous wave EPR spectroscopy. All the pentenyliminyls selectively ring closed in the 5-*exo*-mode rather than the 6-*endo*-mode. EPR monitoring of the decay of the 2,2-dimethyl-1-phenylpent-4-enyliminyl radical showed that it underwent bimolecular combination at about the diffusion controlled limit ($2kt \sim 3 \times 10^8$ M^{-1} s^{-1} at 245 K). The rate constant for 5-*exo*-ring closure of phenylpentenyliminyl (8.8×10^3 s^{-1} at 300 K) was a factor of 25 smaller than the rate constant for hex-5-enyl radical cyclization. The rate of cyclization was slower for an iminyl having a Me group at the site of 5-*exo*-cyclization but faster for an iminyl with an Et substituent at the terminus of the C═C double bond. Surprisingly, the 2,2-dimethyl-1-phenylpent-4-enyliminyl radical, with a bismethyl group in its pentenyl chain, ring closed more slowly than the unsubstituted analogue. DFT computations were in accord with this inverse *gem*-dimethyl effect and suggested it resulted from steric interaction of the Ph and bis-Me groups which forced the aromatic ring out of the plane of the imine moiety. To check on the role of the Ph substituent, pentenyliminyls lacking this group were sought. A pentenyliminyl radical with an alkyl group in place of the Ph group, and a single Me group in its pentenyl chain, was generated by means of an unsymmetrical dioxime oxalate precursor. The k_c for this species was a factor of 2.5 larger than k_c for the original pentenyliminyl, suggesting that the normal positive *gem*-dimethyl effect does operate for pentenyliminyls lacking the aromatic substituent at the C═N bond. DFT computations also successfully reproduced this trend for model iminyls. It appears that for alkenyliminyl radicals positive or negative *gem*-dimethyl effects on the cyclization can be induced by appropriate choice of the second substituent on the C═N bond.

Introduction

Unsaturated iminyl radicals ($R^1R^2C{=}N^{\bullet}$) are known to ring close in 5-*exo* and 6-*endo* modes to give pyrrole and pyridine derivatives, respectively. Preparative procedures incorporating these reactions are steadily becoming more important in syntheses of biologically active aza-heterocycles.[1] Knowledge of the rate constants of iminyl radical cyclizations, and how these vary with structure, would be of intrinsic interest and would be very useful for synthetic planning. However, at present, the only known rate constant is that obtained by Newcomb and co-workers for 5-*exo*-cyclization of the 6,6-diphenylhex-5-en-2-iminyl radical, i.e., 2.2×10^6 s^{-1} at 298 K.[2] This particular cyclization gives rise to a strongly resonance stabilized ring-closed radical containing two phenyl substituents at its radical center. The rate constant for this special case is expected to be considerably larger than that for less substituted analogues.[3] We decided, therefore, to examine the kinetics of ring closures of a set of iminyl radicals that would cover some representative structural features. Although LFP is generally the kinetic method of choice, chromophores adjacent to the cyclized radical center (such as Ph groups) are needed for reliable results. Electron paramagnetic resonance (EPR) spectroscopy is capable of detecting and characterizing N-centered and C-centered radicals without the reporter groups needed for LFP. If both the uncyclized iminyl radical and the cyclized C-centered radical can be simultaneously detected, and their concentrations determined under steady-state conditions, then EPR spectroscopy can be profitably used to determine cyclization rate constants.[4] For EPR spectroscopic studies, alkyliminyl radicals have been generated by addition of electrons to nitriles followed by protonation (or by addition of H-atoms to nitriles),[5] by thermal rearrangements of oxime thionocarbamates,[6] and by H-atom abstraction from imines.[7] The latter study of Griller et al. demonstrated that iminyls terminate by bimolecular combination to give bismethylenehydrazines. The process was found to be fast and diffusion controlled for small iminyls ($2k_t = 4 \times 10^7$, 2×10^8, and 4×10^9 M^{-1} s^{-1} at 238 K for R^1 and R^2 = *i*-Pr, Ph, and CF_3, respectively); i.e., iminyl termination rates were analogous to alkyl radical combination rates. Sterically shielded iminyls like $t\text{-}Bu_2C{=}N^{\bullet}$ terminated much more slowly ($2k_t = 4 \times 10^2$ M^{-1} s^{-1} at 238 K), and at higher temperatures ($T > 248$ K) this species underwent β-scission to give a nitrile and a *t*-Bu radical.

It was shown recently that UV photolysis of oxime esters [$R^1R^2C{=}NOC(O)R$], sensitized with 4-methoxyacetophenone (MAP), is a good way of making iminyl radicals for EPR

* Corresponding author: fax, 44 (0)1334 463808; e-mail, jcw@st-and.ac.uk.
† University of St. Andrews.
‡ Universidad de La Rioja.

10.1021/jp9047902 CCC: $40.75
Published on Web 08/25/2009

spectroscopic study.[8] Furthermore, of this class of compounds, the dioxime oxalates [$R^1R^2C{=}NOC(O)C(O)ON{=}CR^1R^2$], are particularly "clean" precursors yielding only an iminyl and CO_2 on sensitized UV photolysis.[9] It seemed to us that suitably functionalized precursors of these types would be appropriate for a kinetic EPR study of iminyl radical cyclizations. We report such a study in this paper which yielded rate constants and Arrhenius parameters for ring closures of a set of unsaturated iminyl radicals with various structural features. The same reactions were also examined by DFT computational methods enabling the calculated structures and energetics to be compared with the EPR data.

Experimental Section

Materials. 4-Methoxyacetophenone (MAP) and *tert*-butylbenzene were obtained commercially. 2-Phenylbenzaldehyde *O*-acetyloxime, (*Z*)-1-phenyl-4-hepten-1-one *O*-acetyloxime, 1-phenyl-4-penten-1-one *O*-acetyloxime, 1-phenyl-4-penten-1-one *O*-benzoyloxime, 1-phenyl-4-penten-1-one *O*-phenylacetyloxime, (*Z*)-1-(4-methoxyphenyl)-4-hepten-1-one *O*-acetyloxime, and 2,2-dimethyl-1-phenyl-4-penten-1-one *O*-phenylacetyloxime were prepared by standard methods, and details are in the Supporting Information. The dioxime oxalates 1-phenylpent-4-en-1-one dioxime oxalate, 2,2-dimethyl-1-phenylpent-4-en-1-one dioxime oxalate, 4-methyl-1-phenylpent-4-en-1-one dioxime oxalate, 1-(4-methoxyphenyl)pent-4-en-1-one dioxime oxalate, and 1-(2,4-dimethoxyphenyl)pent-4-en-1-one dioxime oxalate were prepared as described previously.[9]

EPR Spectroscopy. EPR spectra were obtained with a Bruker EMX 10/12 spectrometer fitted with a rectangular ER4122 SP resonant cavity and operating at 9.5 GHz with 100 kHz modulation. Solutions of the oxime ester (5−20 mg) and 4-methoxyacetophenone (1 or 2 equiv.) in *tert*-butylbenzene (0.2−0.5 mL) in 4 mm o.d. quartz tubes were deaerated by bubbling nitrogen for 20 min and photolyzed in the resonant cavity by unfiltered light from a 500 W superpressure mercury arc lamp. Solutions in cyclopropane were prepared on a vacuum line by distilling in the cyclopropane, degassing with three freeze−pump−thaw cycles, and finally flame sealing the tubes. In all cases where spectra were obtained, hyperfine splittings (hfs) were assigned with the aid of computer simulations using Bruker SimFonia and NIEHS Winsim2002 software packages. For kinetic measurements, precursor samples were used mainly in "single shot" experiments; i.e., new samples were prepared for each temperature and each concentration to minimize sample depletion effects. In a few cases second shot data were included. EPR signals were double integrated using Bruker WinEPR software, and radical concentrations were calculated by reference to the double integral of the signal from a known concentration of the stable radical DPPH (1×10^{-3} M in PhMe), run under identical conditions, as described previously.[10]

Making the steady-state approximation, the rate equation for reaction of an iminyl radical (im) that takes part in only cyclization (producing radical cy; rate constant k_c) and termination ($2k_t$) processes is given by:[4]

$$k_c/2k_t = [\mathrm{cy}] + [\mathrm{cy}]^2/[\mathrm{im}] \qquad (1)$$

It is necessary therefore to find EPR spectroscopic conditions where both the iminyl and cyclized radical give strong signals that are well enough resolved for double integration and hence for concentration measurements. Previous work had shown that good iminyl signal intensities were only obtained from oxime esters having Ph (or other aromatic) groups attached to their C=N bonds.[8,9] In the first instance, therefore, the acyl oxime ester **1** was photolyzed with MAP in *tert*-butylbenzene as non-H-atom donor solvent. The spectra showed the presence of methyl radicals [a(3H) = 22.8 G], the corresponding iminyl radical (a(N) = 10.1 G, g = 2.0033) together with additional lines for the ring closed dihydropyrrolomethyl radical in the temperature range 230−270 K. However, spectral intensities were poor and overlap with the methyl radical lines obscured the other species.

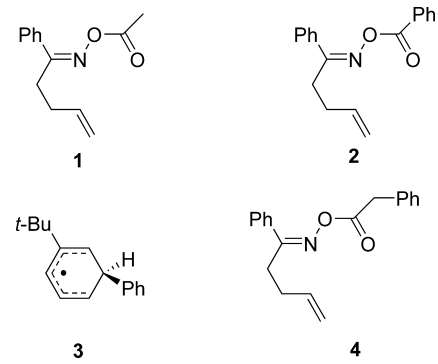

Figure 1. Oxime esters and derived radicals.

Phenyl radicals are generally not detectable by EPR in solution because of their great reactivity, and therefore 1-phenylpent-4-en-1-one *O*-benzoyl oxime (**2**) was prepared and tested. Although the same iminyl radical could be discerned, the spectrum was dominated at most temperatures by a species with a complex signal having five different H-atom hfs, i.e., 35.5, 13.3, 9.3, 8.1, and 2.7 G. We attribute this spectrum to the cyclohexadienyl radical **3** derived from addition of the phenyl radical to the solvent. The benzoyl oxime esters were not therefore suitable precursors. When the phenylacetyl oxime ester **4** was examined, EPR signals from the desired iminyl radical, the cyclized radical, and the benzyl radical (a(2H) = 16.4, a(1H) = 6.2, a(2H) = 5.1, a(2H) = 1.7 G at 225 K) were observed. However, by increasing the microwave power level from 1 to 4 mW the benzyl radical saturated, whereas the iminyl and cyclized species did not. Thus, the spectra from benzyl oxime esters were satisfactorily resolved for kinetic measurements at this microwave power.

We also used a set of dioxime oxalates as precursors. These compounds are potentially better precursors because they initially yield only the desired iminyl radical and CO_2 on sensitized photolysis. However, dioxime oxalates hydrolyze and degrade very easily and most cannot be purified by conventional methods. Traces of oximes from the hydrolysis are difficult to avoid, and these give rise to persistent iminoxyl radical signals in the EPR spectra which can interfere. By careful control of reagent quantities during their preparation, and by using them immediately, satisfactory results were achieved in most cases.

Computational Methods. Radical ground-state calculations were carried out using the Gaussian 03 program package.[11] Becke's three-parameter hybrid exchange potential (B3)[12] was used with the Perdew−Wang (PW91)[13] gradient-corrected correlation functional, B3PW91. This method has proved to describe the chemistry of iminyl radicals accurately.[1] The standard split-valence 6-31+G* basis set was employed. Geometries were fully optimized without any symmetry constraints for all model compounds. Optimized structures were characterized as minima or saddle points by frequency calculations. The experimental kinetic data were all obtained in the nonpolar hydrocarbon solvent *tert*-butylbenzene. Solvent effects,

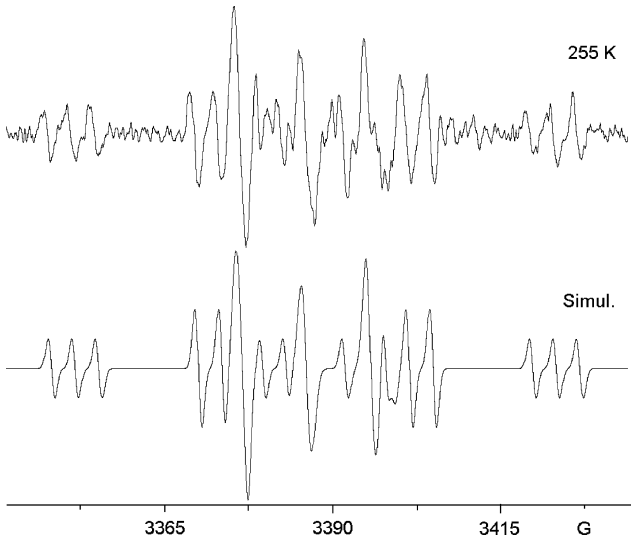

Figure 2. Experimental (top) and simulated (bottom) EPR spectra from photolysis of **5**.

TABLE 1: EPR Parameters of Dihydropyrrolomethyl Radicals 7 in *t*-BuPh Solution[a]

radical	*T*/K	$a(2H_\alpha)$	$a(H_\beta)$	a(N)
7a	250	21.9	28.1	3.7
7b	240	21.9	28.2	3.7
7c	255	21.7	28.7	3.1
7d	275	21.8	*b*	4.3
7e	215	21.0[c]	26.3	4.1
7f	250	21.9	28.9	3.4
7h	255	21.7	28.8	3.5

[a] All *g*-factors 2.0025 ± 0.0001; hfs in gauss. [b] Additional hfs $a(2H) = 0.8$ G. [c] Only $1H_\alpha$, but an additional $a(H_\beta) = 21.0$ G.

particularly differences in solvation between the neutral reactants and neutral transition states, are therefore expected to be minimal. In view of this, no attempt was made to computationally model the effect of the solvent.

Results and Discussion

Generation, EPR Characterization, and Cyclization of Alkenyliminyl Radicals. Photolyses of solutions of either phenylacetyl oxime **4** or the analogous dioxime oxalate **5** with MAP in *tert*-butylbenzene in the temperature range 205−275 K gave rise to EPR spectra from *both* phenylpentenyliminyl **6a** and a second species (Figure 2). The *g*-factor of this second radical (Table 1) showed that it was a C-centered radical. The triplet hfs (21.9 G) was as expected for two α-Hs and the doublet (28.1 G) was appropriate for a β-H atom. This spectrum can therefore, be confidently attributed to the pyrrolomethyl radical **7a** obtained by 5-*exo*-trig ring closure of iminyl **6a**.

The H_β hfs decreased from 29.2 G at 205 K to 28.7 G at 260 K and therefore the preferred, low temperature, conformation of radical **7a** about its $C_\alpha-C_\beta$ bond must be **8** in which H_β eclipses the SOMO (Figure 3).[14] This contrasts with the preferred conformation of the model cyclopentylmethyl radical **9**, but the difference is not surprising in view of the substitution of an N-atom for a CH_2 group at one of the β-positions. In fact, there is practically free rotation about the $C_\alpha-C_\beta$ bond of **7a** as comparison with the ethyl radical shows ($a(H_\beta) = 26.9$ G, independent of *T*)].

The set of substituted iminyl radicals shown in Scheme 2 was generated and their ring closures were examined by EPR spectroscopy. Each of the iminyl radicals was observed to have

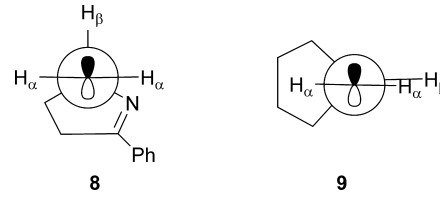

8 **9**

Figure 3. Preferred conformations of dihydropyrrolomethyl and cyclopentylmethyl radicals.

SCHEME 1: Generation and Cyclization of 1-Phenylpent-4-enyliminyl Radical 6a

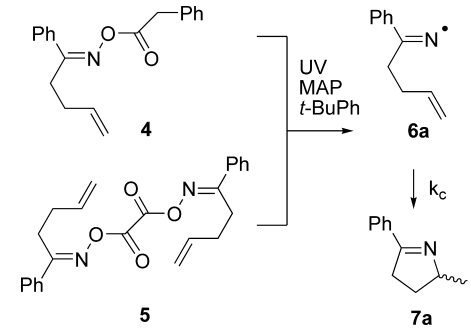

SCHEME 2: Ring Closure of Substituted Iminyl Radicals

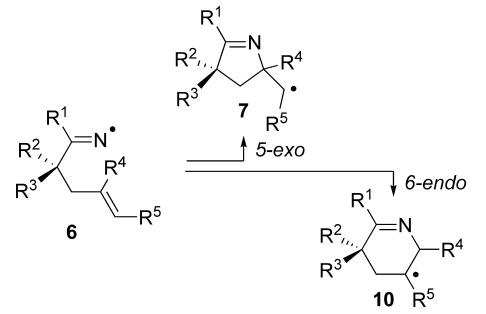

	R^1	R^2	R^3	R^4	R^5	
a	Ph	H	H	H	H	
b	Ar^1	H	H	H	H	Ar^1 = 4-$MeOC_6H_4$
c	Ar^2	H	H	H	H	Ar^2 = 2,4-di$MeOC_6H_3$
d	Ph	H	H	Me	H	
e	Ph	H	H	H	Et	
f	Ph	Me	Me	H	H	
g	H	Me	Me	H	H	
h	CH_2CH_2E	H	Me	H	H	E = CO_2Me

$g = 2.0033 \pm 0.0001$ and a(N) = 10.1 ± 0.03 G. The EPR parameters of the cyclized species are recorded in Table 1 and are consistent in every case with the 5-*exo* ring closure mode to the corresponding pyrrolomethyl radical **7**. Ring closure of the 4-methyl-1-phenylpent-4-enyliminyl **6d** was particularly interesting because, for the model 5-methylhex-5-enyl radical, with a methyl group hindering 5-*exo* approach to the double bond, 6-*endo* ring closure was reported to outweigh 5-*exo* ring closure.[15] The EPR spectra obtained on photolysis of a solution the dioxime oxalate $[PhC(CH_2CH_2CMe{=}CH_2){=}NOC(O)]_2$ and MAP in PhBu-*t* are compared in Figure 4 with a computer simulation containing spectra of both **6d** and **7d**. From this it is evident that the main ring closed species is **7d**. EPR parameters for radicals like **10d** have not been reported, but a DFT computation (B3LYP with a 6-31G(d) basis set) gave $a(H_\alpha) = -22.7$, $a(H_\beta) = 46.5$, 38.3, and 6.9 G. The signals from **10d** should therefore extend well beyond the central region of the spectrum, and if **10d** was formed, its signal would not be

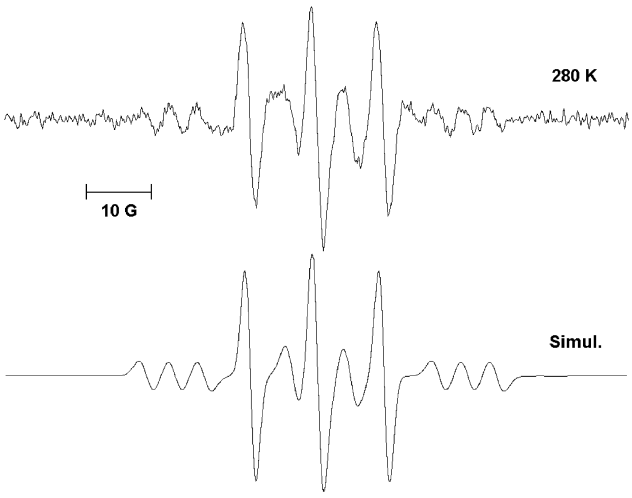

Figure 4. EPR spectra of iminyl **6d** and dihydropyrrolomethyl **7d** in PhBu-*t* at 280 K: top, experimental spectrum; bottom, simulation with parameters for **7d** from Table 1.

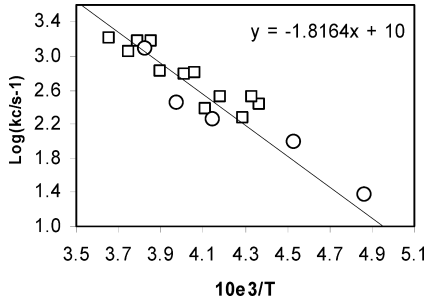

Figure 5. Arrhenius plot of k_c values for radical **6a** with benzyl ester **4** as precursor (□) and with the dioxime oxalate **5** as precursor (○).

completely hidden. Thus, any **10d** is lost in the noise, and we estimated from the signal/noise that [**7d**]/[**10d**] ≥ 4 at 280 K.

Kinetics of Arylpentenyliminyl Radical Cyclizations. The archetype phenylpentenyliminyl radicals **6a** were generated from benzyl ester **4**, and the concentrations of **6a** and **7a** were determined from their EPR spectra in the temperature range 228−272 K. The rate constant ratios $k_c/2k_t$ were derived by use of eq 1. As mentioned above, terminations for sterically unhindered iminyl radicals were found to be fast and diffusion controlled. The diffusion-limited rate constants of small, neutral free radical combination reactions are all the same, to within experimental error, and solvent viscosity is the most important variable. The well-established $2k_t$ rate parameters for *t*-Bu$^{\bullet}$ radicals derived by Fischer and co-workers (log A_t = 11.63 M^{-1} s^{-1}, E_t = 2.25 kcal/mol),[16] corrected for changes in solvent viscosity as described previously,[10,17] were therefore used in the calculation of the absolute k_c values which are plotted in Arrhenius form in Figure 5. As a cross check on the data, and in case residual benzyl radical signals distorted the results, the same iminyl radical was generated from the corresponding dioxime oxalate **5** and radical concentrations measured as before. The good correspondence of the two sets of data (Figure 5) supports the validity of the results. For each iminyl radical the accessible temperature range was small and the error limits on individual rate constants were large. Because of the long extrapolations required, reliable pre-exponential factors could not be derived. Instead, it is well established[3] that the log(*A*) values of *5-exo* cyclizations are close to 10.0 s^{-1}, and therefore this value was used for evaluations of the activation energies in Table 2.

TABLE 2: Rate Parameters for 5-*Exo* Cyclizations of Substituted Iminyl Radicals[a]

radical	source	*T* range (K)	E_c (kcal/mol)	$10^{-3}k_c$ (s^{-1}) (300 K)	*E*[DFT] (kcal/mol)[c]
6a	**4** and **5**	228−272	8.3 ± 1.3	8.8	9.9
6b	sym doo[b]	230−280	9.1 ± 0.9	2.3	
6d	sym doo[b]	270−310	10.7 ± 1.2	0.15	9.8
6e	Me-ester	226−277	7.2 ± 1.0	60	
6f	sym doo[b]	237−285	10.3 ± 1.3	0.31	10.4
6h	**12**	215−260	7.8 ± 2.7	22	

[a] Assumed log(A_c/s^{-1}) = 10.0; error limits are 2σ. [b] Symmetrical dioxime oxalate. [c] B3PW91/6-31+G*.

Previous work had shown that oxime esters with 2- or 4-methoxy substituents in the aromatic rings released iminyl radicals more efficiently on photolysis.[8,9] In an effort to improve the precision of the data, the dioxime oxalate precursor of **6b**, containing a 4-MeO substituent, was prepared and the kinetic results obtained from this precursor are in Table 2. The error limits were slightly improved but not enough to recommend this substitution for general use. For iminyl **6d**, with a Me substituent at the site of 5-*exo* ring closure, the rate was significantly slower and kinetic measurements were carried out at higher temperatures (Table 2). This result is in line with data for analogously substituted hex-5-enyl radicals for which methyl substitution at the radical center also reduces the rate constant for ring closure.[18] An iminyl **6e** with an Et substituent at the terminus of the double bond was also examined. The rate of ring closure was much faster, and consequently the signals from the iminyl radical were weak in the temperature range where *tert*-butylbenzene remained fluid. Reaction of the same precursor in cyclopropane solvent was also examined to try to extend the range of measurements to lower temperatures. Although iminyl **6e** could be clearly identified down to 150 K in this solvent, spectral quality was not good enough for double integrations, probably because of solubility problems. The kinetic data in Table 2 are based on a few spectra in *tert*-butylbenzene solvent. Again, the greater k_c for iminyl **6e** shows the same trend as for cyclizations of hex-5-enyls with alkyl substituents at the terminus of their double bonds.[18]

The results for iminyl **6f**, with *gem*-dimethyl substitution in the pentenyl chain, were particularly interesting. It is known that hex-5-enyl radicals with *gem*-dimethyl substitution at the 2,2′- and 3,3′- and 4,4′-positions ring close with rate constants more than an order of magnitude greater (>by factors of 15, 22, and 14, respectively) than the unsubstituted hex-5-enyl [k_c (298 K) = 2.3 × 10^5 s^{-1}].[18−20] We expected therefore that **6f** would ring close more rapidly than **6a** due to a *gem*-dimethyl effect. Surprisingly, the measured rate constant for **6f** cyclization at 300 K was significantly smaller than that of **6a** (by a factor of 28) and the activation energy of the process was higher (Table 2).

The radical center in iminyl **6f** has adjacent Ph and bis-Me substituents which might have hindered the dimerization process such that smaller $2k_t$ values would be appropriate.[21] The decay of the EPR signal of **6f** as a function of time was therefore investigated. Ideally, for $2k_t$ measurements, the decay should be recorded at temperatures where no first-order cyclization complicates the mechanism. However, at the low temperatures where cyclization was negligible, the iminyl signals were broadened due to anisotropic radical tumbling and were not sufficiently intense for decay measurements. The best compromise was at 245 K where good signal intensity led to reasonable decay kinetics. Figure 6 shows the EPR spectrum at this

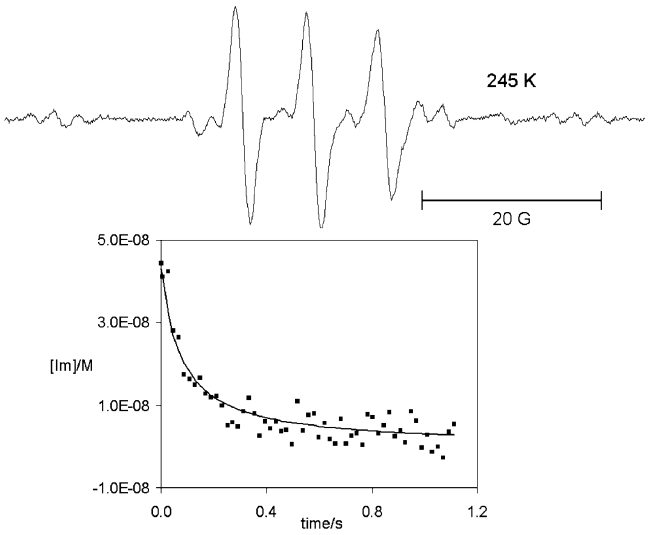

Figure 6. EPR spectrum and decay curve of iminyl radical **6f** at 245 K.

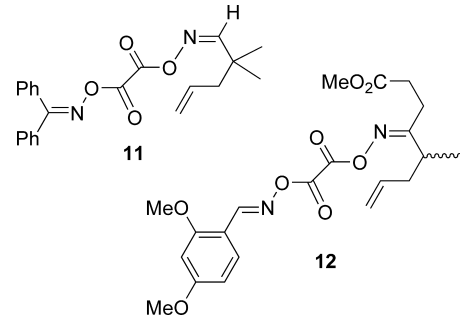

Figure 7. Unsymmetrical dioxime oxalates for generating iminyl radicals without aromatic substituents.

TABLE 3: Computed Energy Barriers for 5-*Exo* Cyclizations of 6a Using Different Functionals

functional	energy barrier (kcal/mol)
B3PW91	9.9
B3LYP	11.6
SVWN	2.1
BLYP	10.2

temperature with the iminyl decay curve for an initial $[\mathbf{6f}]_i = 4.3 \times 10^{-8}$ M.

The ratio [**6f**]/[**7f**] $\sim$ 6 at this temperature, so there was undoubtedly a minor first-order contribution to the decay under these conditions. However, a second-order decay curve with $2k_t = 3 \times 10^8$ M^{-1} s^{-1} fitted the experimental data well (Figure 6). The large magnitude of this rate constant shows the termination of **6f** was extremely rapid and probably diffusion controlled, like the other small iminyls. In view of the undoubted first-order contamination, the measured $2k_t$ will only be a rough estimate. The more reliable data of Fischer was therefore used for $2k_t$ in the calculation of the cyclization coefficients of Table 2.

It is safe to conclude that ring closure of iminyl **6f** shows an *inverse gem*-dimethyl effect. This is unusual because not only hex-5-enyl radical cyclizations but also many other ring closure processes are known to be accelerated by gem-disubstituent effects.[16,22] Some exceptions are, however, known.[23]

Kinetics of Cyclization of a Nonaromatic Pentenyliminyl Radical. One of the main differences between iminyls **6a**−**f** and the corresponding hex-5-enyls is the presence of the Ph substituent on their C═N bonds close to their radical centers. It seemed important to establish if ring closures of iminyl radicals lacking this Ph substituent were subject to a *gem*-dimethyl effect. As mentioned above, photolyses of oxime esters and dioxime oxalates only proceed sufficiently well for EPR study of the released radicals if an aromatic substituent is present. To overcome this problem we prepared the unsymmetrical dioxime oxalates **11** and **12** which contain aromatic substituents at one end and suitably substituted iminyl groups at the other end (Figure 7).

Fresh samples of compound **11** were photolyzed with MAP in the EPR resonant cavity, but unfortunately the spectra were dominated by large signals from an unknown persistent radical. This occurred even when NMR spectra showed **11** to be pure. It seems that **11** takes part in some alternative degradative process during UV irradiation. On the other hand, photolysis of compound **12** gave rise to EPR signals from the 2,4-dimethoxyphenyliminyl radical ($g = 2.0034$, $a(N) = 10.1$ G, $a(1H) = 81.2$ G) which were well separated from the spectra of iminyl **6h** and dihydropyrrolomethyl **7h** because of the large hfs from the single H-atom. The ring closure of **6h** took place at the lower end of the temperature range of *t*-BuPh solvent, where anisotropic line broadening occurs, so the data are less accurate, but they clearly show that the single Me substituent caused a significant increase in the rate constant for iminyl ring closure. For model hex-5-enyl radical cyclizations the rate constants for the mono-3-methyl substituted radical are intermediate between that of the unsubstituted parent radical and that of the *gem*-3,3′-dimethyl substituted radical.[24] Our data are good evidence therefore that iminyl radicals without aryl substituents on the C═N bond would show the normal positive *gem*-dimethyl effect.

Theoretical Calculations. In order to shed some light on the ring-closure process, we decided to study the cyclization by means of theoretical calculations. Our first task was to test some levels of theory using the experimental data for cyclization of **6a** as the benchmark. As mentioned before (see Figure 5 and Table 2), the 5-*exo* cyclization of **6a** exhibited a value for E_c of 8.3 $\pm$ 1.3 kcal/mol, assuming $\log(A/s^{-1}) = 10.0$. We therefore took this value as a good approximation of the real value and used it to validate our theoretical approach. We performed a series of calculations on the 5-*exo* cyclization of **6a** to evaluate the performance of a set of different functionals using the standard 6-31+G* basis set. Results are shown in Table 3. In every case, the structures for both the minimum and transition state remained very similar, and only the relative energies changed.

As can be seen, both the B3PW91 and BLYP functionals gave results in reasonable agreement with experiment. From these two options, we started by using hybrid functional B3PW91 together with the standard basis set 6-31+G*, as this combination gave results in agreement with experiment and it has also been successfully used before in the description of iminyl radicals.[1] In order to explore the effect of the basis set on the computed barrier, we re-evaluated the transition structure using two larger basis sets, namely, the triple split valence basis 6-31+G(d,p) and the correlation consistent polarized triple-ζ basis set, cc-pVTZ. The computed energy barriers were 10.4 and 10.2 kcal/mol, respectively. As can be seen, no significant improvement in the results was obtained using these larger basis sets, although the time required to complete the calculations was considerably longer. With these data in hand, we decided to use the standard 6-31+G* basis set in further calculations.

Next, we explored the performance of Møller−Plesset perturbation theory in the description of the ring-closure process.

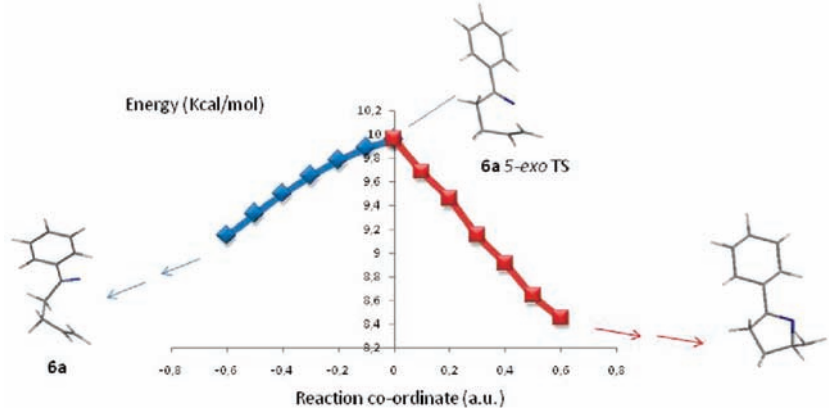

Figure 8. Reaction path for the 5-*exo* cyclization for radical **6a**.

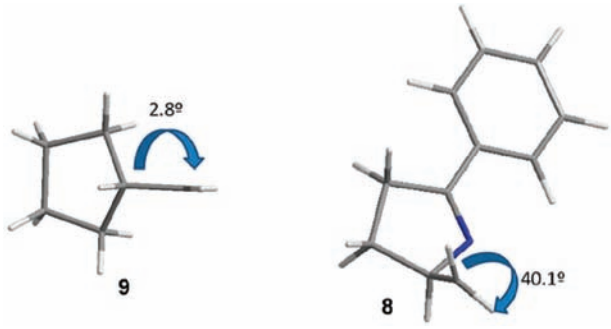

Figure 9. Computed conformations for cyclopentylmethyl **9** and dihydropyrrolomethyl radicals **8**.

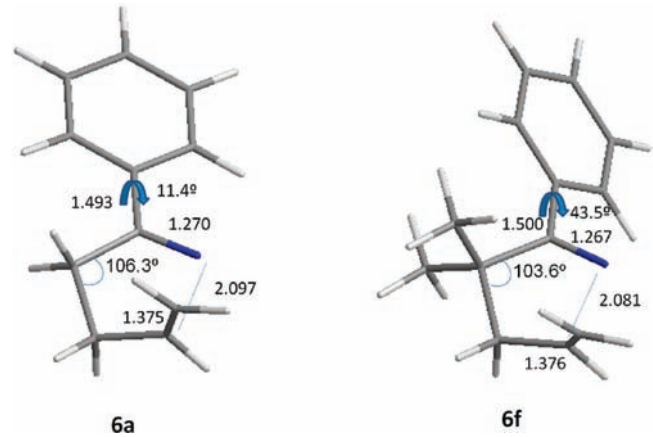

Figure 10. Transition structures for the 5-*exo* ring closures of **6a** and **6f**. Distances in angstroms and angles in degrees.

We computed the cyclization barrier for **6a** using MP2, MP3, and MP4 together with the 6-31+G* basis set. We observed that absolute energies showed oscillation as a function of the perturbation order. This behavior is quite usual because a smooth convergence is only expected in systems with well-separated electron pairs.[25] The presence of lone pairs and multiple bonds in the systems explored makes the oscillation behavior of the total energy natural. However, as only the relative energies are relevant to the study of the cyclization process, we completed the study of the ring closure process. We obtained values for the energy barrier of 22.0, 18.9, and 19.8 kcal/mol for MP2, MP3, and MP4, respectively. These results were much higher than the experimental value, so we decided to take the hybrid functional B3PW91 together with the 6-31+G* basis sets as our standard for further calculations.

We also checked the nature of the transition structure for the 5-*exo* cyclization of **6a** through an IRC computation. The results are shown in Figure 8.

Having assessed the performance of the model theories, we aimed to study the computed ground state and transition state structures. Figure 9 shows the calculated geometries for **8** and **9**. As expected from the EPR data for cyclopentylmethyl **9** (see above), H_β lies in the same plane as both H_α atoms (dihedral angle $H_\beta-C-C-H_\alpha = 2.8°$). However, substitution of a methylene group by an N-atom in dihydropyrrolomethyl radical **8** leads to a preferred dihedral angle of 40.1°, again in reasonable agreement with the EPR data.

For **6a** both the 5-*exo* vs the 6-*endo* ring closure processes were explored and the transition structures leading to the five and six-membered species were computed. As expected, the 5-*exo* ring closure was found to be kinetically favored with an energy barrier of 9.9 kcal/mol as compared with the barrier for the 6-*endo* cyclization which was found to be 13.6 kcal/mol. This is in agreement with the experimental results (see above) because only **6a** and **7a** were detected. Similarly, **6d** was experimentally found to give **7d** while **10d** was not detected. Our calculations show that the energy barrier leading to **7d** (5-*exo* ring closure) is 9.8 while the corresponding barrier to **10d** (6-*endo*) is 11.5. Thus, while the 5-*exo* process is still kinetically favored, the energy difference between the two paths is smaller for **6d** (1.7 kcal/mol) than for **6a** (3.7 kcal/mol).

As shown above, **6f** was expected to ring close more rapidly than **6a** due to the same *gem*-dimethyl effect observed in substituted hex-5-enyl radicals. However, experimentally, a considerably *smaller* rate constant was found for **6f** than for **6a**. We therefore explored the reaction of **6f** trying to find an explanation for the lack of *gem*-dimethyl effect. As mentioned before, the transition structure for 5-*exo* cyclization of **6a** lies 9.9 kcal/mol above the **6a** minimum, while the corresponding structure for **6f** was found to be 10.4 kcal/mol higher in energy than **6f**. These results were in agreement with the experimental data as **6f** shows a higher energy barrier for the ring closure consistent with the smaller rate constants experimentally measured. Analysis of the computed structures (Figure 10) allowed us to draw some conclusions.

The main geometrical difference between both transition structures is the dihedral angle connecting the aromatic ring and the imine moiety. While in **6a** this dihedral angle is small (11.4°) reflecting the coplanar relationship between both groups, the presence of two methyl groups in **6f** causes an increase in the dihedral angle (43.5°) due to steric hindrance. The presence of two methyl groups also contributes to a decrease in the C−C−C angle (106.3° in **6a** and 103.6° in **6f**) as expected.

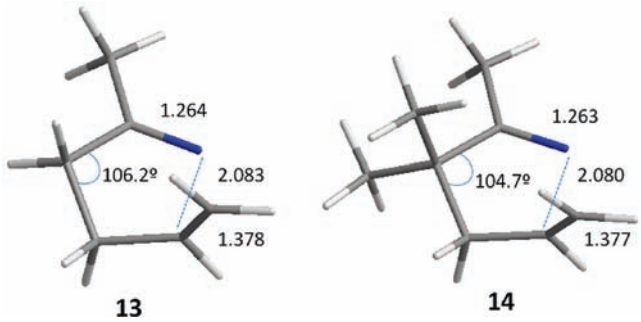

Figure 11. Computed transition structures for 5-*exo* ring closures for nonaromatic iminyl radicals **13** and **14**.

TABLE 4: Computed Energy Barriers for 5-*Exo* and 6-*Endo* Cyclizations of 6d and 15

radical	cyclization	energy barrier (kcal/mol)
6d	5-*exo*	9.8
6d	6-*endo*	11.5
15	5-*exo*	9.0
15	6-*endo*	8.5

These changes, although small, contribute to a higher energy barrier for ring closure and the reversal of the *gem*-dimethyl effect.

However, we also showed that nonaromatic pentenyliminyl radicals do show the positive *gem*-dimethyl effect as confirmed by photolysis of **12**. We chose to compute the 5-*exo* ring closures for **13** and **14** (see Figure 11) as models for nonaromatic iminyls.

The computed barriers for the 5-*exo* ring closure were 10.8 kcal/mol for **13** and 10.2 kcal/mol for **14**. Thus, **14** is expected to ring close faster than **13** in accordance with the presence of a *gem*-dimethyl effect. As our computations show, the change of the phenyl ring in **6a** and **6f** for a methyl group in **13** and **14** leads to a decrease in the steric hindrance. Thus, the methyl groups play a prominent role in the case of nonaromatic iminyl radicals. Computational data are in good agreement with experimental data as they predict a reverse *gem*-dimethyl effect when it comes to aryl-iminyl radicals, while nonaromatic iminyl radicals follow the same pattern as model hex-5-enyl radicals.

In this context, it seemed useful to directly compare the behavior of iminyl radicals with hex-5-enyl radicals. As noted before, the model 5-methylhex-5-enyl radical was reported to follow a 6-*endo* ring closure instead of 5-*exo*.[15] However, the similar iminyl radical **6d** yielded mainly **7d** through a 5-*exo* approach. In order to clarify this question, we computed both approaches (i.e., 5-*exo* and 6-*endo* ring closures) for **6d** and **15** (5-methyl-2-phenylhex-5-enyl radical). Results are shown in Table 4 and Figure 12.

The different experimental behavior found for **6d** and **15** was well reproduced by the theoretical calculations. For iminyl radical **6d** the 5-*exo* ring closure was found to proceed faster with a smaller energy barrier. In the case of the C-analogue **15**, the energy difference between both paths is quite small, but the final result is in agreement with experiment because the 6-*endo* ring closure shows a smaller energy barrier. A possible explanation for these results can be obtained from the computed structures. For **6d**, the 6-*endo* ring closure proceeds through a transition structure with the methyl group in a *pseudoaxial* position, eclipsed with the adjacent H atom, together with a slighter bigger distortion of the angles (123.4° for the N═C—C angle, 120° in the radical minimum). This distortion is smaller in the 5-*exo* ring closure (118.4°). The absence of a C═N double

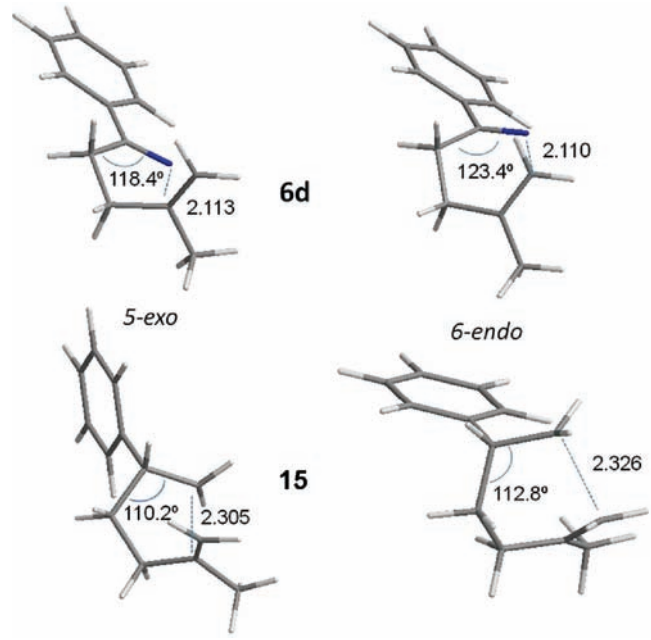

Figure 12. Computed transition structures for 5-*exo* and 6-*endo* cyclizations of **6d** and **15**.

bond in **15** leads to less strained transition structures. In this case, the 5-*exo* approach requires a higher distortion (110.2° compared with the radical minimum 113.5°) than the 6-*endo* ring closure (112.8°) which could explain the preference for the latter.

Conclusions

Two types of pentenyliminyl radicals were studied: the first with aryl substituents at their C═N bonds and one of a second type with an alkyl substituent at its C═N bond. Both types of radicals selectively ring closed in the 5-*exo* mode, irrespective of the substitution pattern around the C═C double bond of the pentenyl chain. The rapid decay of the 2,2-dimethyl-1-phenylpent-4-enyliminyl radical **6f** showed that termination was mainly bimolecular and took place at the diffusion-controlled limit, as observed for most small C- and N-centered radicals. In view of this, study of the kinetics of iminyl cyclizations by the usual steady state EPR method was justified. For archetype phenylpentenyliminyl **6a** the rate constant for 5-*exo* ring closure (8.8×10^3 s^{-1} at 300 K) was a factor of 25 less than the rate constant for hex-5-enyl radical cyclization. This is in very good accord with Newcomb's data for the 6,6-diphenylhex-5-en-2-iminyl radical for which k_c was found to be a factor of 23 less than k_c for the analogously substituted hex-5-enyl radical.[26] A pentenyliminyl with a Me group at the site of 5-*exo* cyclization **6d**, ring closed more *slowly* than **6a** by a factor of ca. 68 whereas pentenyliminyl **6e**, with an Et group at the terminus of the C═C double bond, ring closed *faster* than **6a** by a factor of ca. 7. These trends followed the same SAR pattern as for hex-5-enyl type radicals. Unexpectedly, in comparison with hex-5-enyl analogues, the 2,2-dimethyl-1-phenylpent-4-enyliminyl radical **6f** ring closed more slowly than that of **6a**. The k_c ratio for **6f/6a** was 0.035, which indicated a substantial *inverse gem*-dimethyl effect. DFT computations were in accord with this inverse *gem*-dimethyl effect and suggested it resulted from steric interaction of the Ph and bis-Me groups which pushed the aromatic ring out of the plane of the imine moiety by 43.5°. To check on the role of the Ph substituent, pentenyliminyls lacking this group were sought. Although we were not able to study

the simplest, 2,2-dimethylpentenyliminyl **6g** due to a competing process, the alkyl-substituted radical **6h** containing a single Me substituent in the pentenyl chain was successfully generated from unsymmetrical dioxime oxalate **12**. The k_c for this species was a factor of 2.5 larger than k_c for **6a** suggesting that the normal positive *gem*-dimethyl effect does operate for pentenyliminyls lacking the aromatic substituent at the C═N bond. Our DFT computations also successfully reproduced this trend for model iminyls **13** and **14** (see Figure 11). To our knowledge this is the first example of a *gem*-dimethyl effect which can be inverted by changing the substituent on the C-atom adjacent to the CMe_2 group from alkyl to aryl. Evidently, it is no longer appropriate to make broad generalizations about bis-methyl groups accelerating ring closure reactions.

Acknowledgment. We thank EPSRC (HIPER basic technology project) and EaStChem for financial support. R.A. thanks the Comunidad Autónoma de La Rioja for his fellowship and D.S. thanks the "Ramón y Cajal" program from the MICINN.

Supporting Information Available: Details of oxime ester preparations, tables of radical concentrations and rate constant ratios, ^{1}H and ^{13}C NMR spectra for new compounds, and Cartesian coordinates for the calculated geometries. This material is available free of charge via the Internet at http://pubs.acs.org.

References and Notes

(1) Forrester, A. R.; Gill, M.; Meyer, C. J.; Sadd, J. S.; Thomson, R. H. *J. Chem. Soc., Perkin Trans. 1* **1979**, *60*, 6–611. Forrester, A. R.; Gill, M.; Sadd, J. S.; Thomson, R. H. *J. Chem. Soc., Perkin Trans. 1* **1979**, 612–615. Forrester, A. R.; Gill, M.; Thomson, R. H. *J. Chem. Soc., Perkin Trans. 1* **1979**, 616–620. Forrester, A. R.; Napier, R. J.; Thomson, R. H. *J. Chem. Soc., Perkin Trans. 1* **1981**, 984–987. Zard, S. Z. *Synlett* **1996**, 1148–1154. Kaim, L. E.; Meyer, C. *J. Org. Chem.* **1996**, *61*, 1556–1557. Takai, K.; Katsura, N.; Kunisada, Y. *Chem. Commun* **2001**, 1724–1725. Bowman, W. R.; Bridge, C. F.; Brookes, P.; Cloonan, M. O.; Leach, D. R. *J. Chem. Soc., Perkin Trans. 1* **2002**, 58–68. Bowman, W. R.; Cloonan, M. O.; Fletcher, A. J.; Stein, T. *Org. Biomol. Chem* **2005**, *3*, 1460–1467. Boivin, J.; Fouquet, E.; Zard, S. Z. *Tetrahedron Lett.* **1991**, *32*, 4299–4302. Boivin, J.; Schiano, A.-M.; Zard, S. Z. *Tetrahedron Lett.* **1992**, *33*, 7849–7852. Alonso, R.; Campos, P. J.; Garcia, B.; Rodriguez, M. A. *Org. Lett.* **2006**, *8*, 3521–3523. Alonso, R.; Campos, P. J.; Rodrýguez, M. A.; Sampedro, D. *J. Org. Chem.* **2008**, *73*, 2234–2239.

(2) Le Tadic-Biadatti, M.-H.; Callier-Dublanchlet, A.-C.; Horner, J. H.; Quiclet-Sire, B.; Zard, S. Z.; Newcomb, M. *J. Org. Chem.* **1997**, *62*, 559–563.

(3) Horner, J. H.; Musa, O. M.; Bouvier, A.; Newcomb, M. *J. Am. Chem. Soc.* **1998**, *120*, 7738–7748.

(4) Griller, D.; Ingold, K. U. *Acc. Chem. Res.* **1980**, *13*, 200–206. Griller, D.; Ingold, K. U. *Acc. Chem. Res.* **1980**, *13*, 317–323.

(5) Neta, P.; Fessenden, R. W. *J. Phys. Chem.* **1970**, *74*, 3362–3365.

(6) Hudson, R. F.; Lawson, A. J.; Lucken, E. A. C. *J. Chem. Soc., Chem. Commun.* **1971**, 808–809. Hudson, R. F.; Lawson, A. J.; Record, K. A. F. *J. Chem. Soc., Chem. Commun* **1974**, 488–489.

(7) Griller, D.; Mendenhall, G. D.; Van Hoof, W.; Ingold, K. U. *J. Am. Chem. Soc.* **1974**, *96*, 6068–6070.

(8) McCarroll, A. J.; Walton, J. C. *J. Chem. Soc., Perkin Trans. 2.* **2000**, 2399–2409.

(9) Portela-Cubillo, F.; Scanlan, E. M.; Scott, J. S.; Walton, J. C. *Chem Commun.* **2008**, 4189–4191. Portela-Cubillo, F.; Lymer, J.; Scanlan, E. M.; Scott, J. S.; Walton, J. C. *Tetrahedron* **2008**, *64*, 11908–11916.

(10) Maillard, B.; Walton, J. C. *J. Chem. Soc., Perkin Trans. 2* **1985**, 443–450.

(11) Frisch, M. J. Trucks, G. W.; Schlegel, H. B.; Scuseria, G. E.; Robb, M. A.; Cheeseman, J. R.; Montgomery, J. A.; Vreven, T.; Kudin, K. N.; Burant, J. C.; Millam, J. M.; Iyengar, S. S.; Tomasi, J.; Barone, V.; Mennucci, B.; Cossi, M.; Scalmani, G.; Rega, N.; Petersson, G. A.; Nakatsuji, H.; Hada, M.; Ehara, M.; Toyota, K.; Fukuda, R.; Hasegawa, J.; Ishida, M.; Nakajima, T.; Honda, Y.; Kitao, O.; Nakai, H.; Klene, M.; Li, X.; Knox, J. E.; Hratchian, H. P.; Cross, J. B.; Bakken, V.; Adamo, C.; Jaramillo, J.; Gomperts, R.; Stratmann, R. E.; Yazyev, O.; Austin, A. J.; Cammi, R.; Pomelli, C.; Ochterski, J. W.; Ayala, P. Y.; Morokuma, K.; Voth, G. A.; Salvador, P.; Dannenberg, J. J.; Zakrzewski, V. G.; Dapprich, S.; Daniels, A. D.; Strain, M. C.; Farkas, O.; Malick, D. K.; Rabuck, A. D.; Raghavachari, K.; Foresman, J. B.; Ortiz, J. V.; Cui, Q.; Baboul, A. G.; Clifford, S.; Cioslowski, J.; Stefanov, B. B.; Liu, G.; Liashenko, A.; Piskorz, P.; Komaromi, I.; Martin, R. L.; Fox, D. J.; Keith, T.; Al-Laham, M. A.; Peng, C. Y.; Nanayakkara, A.; Challacombe, M.; Gill, P. M. W.; Johnson, B.; Chen, W.; Wong, M. W.; Gonzalez, C.; Pople, J. A. *Gaussian 03, Revision C.02*; Gaussian, Inc.: Wallingford, CT, 2004.

(12) Becke, A. D. *J. Chem. Phys.* **1993**, *98*, 5648–5652.

(13) Perdew, J. P.; Burke, K.; Wang, Y. *Phys. Rev. B* **1996**, *54*, 16533–16539.

(14) Kemball, M. L.; Walton, J. C.; Ingold, K. U. *J.Chem. Soc., Perkin Trans. 2.* **1982**, 1017–1023. Krusic, P. J.; Meakin, P.; Jesson, J. P. *J. Phys. Chem.* **1971**, *75*, 3438–3453. Kochi, J. K. *Adv. Free-Radical Chem.* **1975**, *5*, 189–317.

(15) Beckwith, A. L. J.; Blair, I. A.; Phillipou, G. *Tetrahedron Lett.* **1974**, 2251–2254.

(16) Schuh, H.-H.; Fischer, H. *Helv. Chim. Acta* **1978**, *61*, 2130–2164. Schuh, H.-H.; Fischer, H. *Int. J. Chem. Kinet.* **1976**, *8*, 341–356.

(17) Bella, A. F.; Jackson, L. V.; Walton, J. C. *J. Chem. Soc., Perkin Trans. 2* **2002**, 1839–1843.

(18) (a) Beckwith, A. L. J.; Ingold, K. U. In *Rearrangements in Ground and Excited States*; Academic Press: New York, 1980; Chapter 4, pp 161−310. (b) Beckwith, A. L. J.; Easton, C. J.; Lawrence, T.; Serelis, A. K. *Aust. J. Chem.* **1983**, *36*, 545–556. (c) Newcomb, M. *Tetrahedron* **1993**, *49*, 1151–1176.

(19) Johnston, L. J.; Lusztyk, J.; Wayner, D. D. M.; Abeywickreyma, A. N.; Beckwith, A. L. J.; Scaiano, J. C.; Ingold, K. U. *J. Am. Chem. Soc.* **1985**, *107*, 4594–4596.

(20) Jung, M. E.; Piizzi, G. *Chem. Rev.* **2005**, *105*, 1735–1766.

(21) Of course, slower termination would not explain the comparatively slow cyclization of **6f**. The EPR method measures $k_c/2k_t$ values and hence smaller $2k_t$ would lead to *smaller* k_c values.

(22) Kaneti, J.; Kirby, A. J.; Koedjikov, A. H.; Pojarlieff, I. G. *Org. Biomol. Chem.* **2004**, *2*, 1098–1103. Lightstone, F. C.; Bruice, T. C. *J. Am. Chem. Soc.* **1994**, *116*, 10789–10790.

(23) Kim, Y. J.; Grimm, J. B.; Lee, D. *Tetrahedron Lett.* **2007**, *48*, 7961–7964.

(24) Beckwith, A. L. J.; Lawrence, T.; Serelis, A. K. *Chem. Commun.* **1980**, 484–485.

(25) Jensen, F. *Introduction to Computational Chemistry*; Wiley: New York, 1999; p 130.

(26) Fallis, A. G.; Brinza, I. M. *Tetrahedron* **1997**, *53*, 17543–17595.

JP9047902